Preamble. This is a reprint of the article:

M. Schulze Darup and J. Renner. Predictive pressure control in deep geothermal systems. In *Proc. of the 2016 European Control Conference*, pp. 605–610, 2016.

Predictive pressure control in deep geothermal systems

Moritz Schulze Darup[†] *and* Jörg Renner[‡]

Abstract

We present a predictive control scheme to regulate the fluid pressure in the reservoir rock of deep geothermal systems. Controlling the fluid pressure profile is important to avoid strong seismic events during hydraulic stimulation. The introduced predictive controller builds on a nonlinear, uncertain, and non-differentiable model describing the pressurization and seismicity in the reservoir. Since measurements of system states are limited, we additionally design an unscented Kalman filter to solve the observation problem.

1 Introduction

Geothermal systems become more and more important for the generation of electrical energy. The total worldwide installed capacity of geothermal power plants currently is 12.635 GW with an increase of about 350 MW per year (see [1] for details). Geothermal power plants are, in general, environmentally friendly. However, the development of enhanced geothermal systems (EGS, see Fig. 1) requires to artificially increase the permeability in the reservoir rock such that water can circulate. The permeability increase is effectuated by hydraulic stimulation that causes seismic activity. While the magnitudes of the induced seismic events are typically small, strong events were recognized during some hydraulic stimulations (see, e.g., Tab. 1 or [2]). Although such induced seismicity is usually short lived, the activities in Soultz and Basel have raised public concern due to their proximity to populated areas. The goal is thus to safely develop an EGS without provoking massive seismicity.

In this paper, we introduce a predictive control scheme to regulate the fluid pressure profile in the reservoir rock of an EGS. Controlling the pressure profile is the key to manage the induced seismicity. We stress, however, that the presented method is not yet capable of directly regulating the seismi-city. The procedure to be presented should thus be understood as a preparatory work for a more complex predictive control scheme explicitly including the induced seismicity. We refer to [3] for a first approach towards the active regulation of seismic activity during hydraulic stimulation.

[†] M. Schulze Darup is with the Control Group, Department of Engineering Science, University of Oxford, Parks Road, Oxford OX1 3PJ, UK. E-mail: moritz.schulzedarup@rub.de.

[‡] J. Renner is with Experimental Geophysics, Department of Geoscience, Ruhr-Universität Bochum, Germany. E-mail: joerg.renner@rub.de.

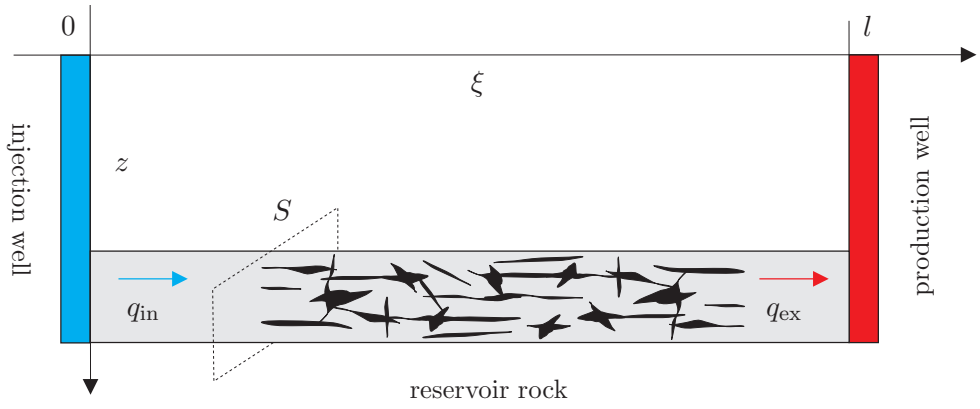

Figure 1: Schematic illustration of an enhanced geothermal system. The injected water is heated up in the reservoir rock and extracted through the production well. The permeability in the reservoir can be artificially increased by hydraulic stimulations causing the creation of new and the extension of existent fractures.

In principle, the fluid pressure in the reservoir rock can be controlled by adapting the fluid flow in two wells (that, during power plant operation, will serve as injection and production well). The pressurization in the reservoir will be delayed and alleviated due to diffusion processes. We thus consider a model predictive control (MPC) scheme to account for this behavior. The repeated solution of the underlying optimal control problem (OCP) requires the knowledge of (an estimation of) the current system state. Since it is not possible to completely measure the system state (including pressures, permeabilities, and stresses), the design of an state observer is required. We implement an unscented Kalman Filter (UKF) for this purpose since the considered model of an EGS is nonlinear, uncertain, and non-differentiable.

Table 1: Maximum magnitude earthquakes induced by fluid injection.

Location	Magnitude	Year	Reference
Soultz-sous-Forêts (France)	2.9	2003	[2, Tab. 1]
Basel (Switzerland)	3.4	2006	[2, Tab. 1]
Cooper Basin (Australia)	3.7	2003	[2, Tab. 1]
Berlín Field (El Salvador)	4.4	2003	[4, Tab. 1]

The paper is organized as follows. We state basic notation in the remainder of this section. In Section 2, we introduce a rudimentary model (that is inspired by [4]) to describe the pressurization and seismic activity in an EGS. We analyze the derived model in Section 3 and show that elementary characteristics of an EGS are reproduced by the model. The main result of the paper, i.e., the predictive pressure control and state observation for an EGS, is presented in Section 4. Finally, conclusions are stated in Section 5.

1.1 Notation

We denote reals, positive reals, and natural numbers (including 0) by $\mathbb{R}$, $\mathbb{R}_+$, and $\mathbb{N}$, respectively. In addition, we define $\mathbb{N}_{[i,k]} := \{j \in \mathbb{N} \,|\, i \leq j \leq k\}$. Beside the Euclidean vector norm $\|x\|_2$, we frequently use $\|x\|_P := \sqrt{x^T P x}$, where P is a positive semi-definite

square matrix. We write $\mathrm{diag}(d_1, \ldots, d_n)$ for a diagonal matrix with elements $d_1 \in \mathbb{R}$ through $d_n \in \mathbb{R}$ on its main diagonal. Finally, $\mathcal{N}(v, \varsigma^2)$ denotes a normal distribution with expectation $v \in \mathbb{R}$ and standard deviation $\varsigma \in \mathbb{R}_+$.

2 Modeling the fluid pressure

2.1 Diffusion equation and Darcy's law

The spatial and temporal evolution of the fluid pressure $p(\xi, t)$ in the reservoir can be approximately described by the diffusion equation

$$\frac{\partial p(\xi,t)}{\partial t} = \frac{\kappa(\xi,t)}{\zeta\eta}\,\frac{\partial^2 p(\xi,t)}{\partial \xi^2}, \tag{1}$$

where ζ is the specific storage capacity, η is the fluid viscosity and κ is the (spatially and temporally varying) rock permeability (see, e.g., [5, p. 215 and p. 340] or [6]). Using Darcy's law (see, e.g., [5, p. 119 ff.]), the injected and extracted fluid at the boundaries result in (Neumann) boundary conditions of the form

$$\frac{\partial p(0,t)}{\partial \xi} = -\frac{\eta\, q_{\mathrm{in}}(t)}{S\,\kappa(0,t)} \quad \text{and} \quad \frac{\partial p(l,t)}{\partial \xi} = -\frac{\eta\, q_{\mathrm{ex}}(t)}{S\,\kappa(l,t)}, \tag{2}$$

where S refers to the cross section of the reservoir (see Fig. 1). The initial-boundary value problem is completed by the initial condition $p(\xi, 0) = p^*$, where p^* is the hydrostatic fluid pressure depending on the depth of the reservoir.

2.2 Discretization

The partial differential equation (1) can be easily discretized using finite differences. However, taking into account that the permeability (and therefore the hydraulic diffusivity $\Lambda := \kappa/\zeta\eta$) is affected by spatial and temporal variations, conventional forward Euler, backward Euler, or Crank-Nicolson schemes are not suitable. Following [5, Eq. (7.9.8)], we consequently use the adapted scheme

$$\sum_{\Delta j=-1}^{1} \alpha_{\Delta j}\,\frac{p_{j+\Delta j}^{k+1} - p_{j+\Delta j}^{k}}{\kappa_{j+\Delta j}^{k+1}\,\Delta t} = \sum_{\Delta k=0}^{1} \frac{p_{j-1}^{k+\Delta k} - 2\,p_{j}^{k+\Delta k} + p_{j+1}^{k+\Delta k}}{\zeta\,\eta\,\Delta\xi^2}, \tag{3}$$

where $p_j^k := p(\xi_j, t_k)$ and $\kappa_j^k := \kappa(\xi_j, t_k)$ with $\xi_j := j\Delta\xi$ and $t_k := k\,\Delta t$, and where $\Delta\xi$ and Δt denote the spatial[1] and temporal step sizes, respectively. Following [5, Eq. (7.9.8)], we chose the weights

$$\alpha_{-1} := 1/6, \qquad \alpha_0 := 5/3, \quad \text{and} \quad \alpha_1 := 1/6.$$

Clearly, (3) can only be applied to inner nodes of the discretization grid and thus does not apply for $j \in \{0, \nu\}$, where $\nu := l/\Delta\xi$. However, for the outer nodes, we obtain

$$q_i^k = \frac{S\,\kappa_0^{k+1}}{\eta}\,\frac{3\,p_0^{k+1} - 4\,p_1^{k+1} + p_2^{k+1}}{2\,\Delta\xi} \quad \text{and} \tag{4}$$

$$q_e^k = \frac{S\,\kappa_\nu^{k+1}}{\eta}\,\frac{-p_{\nu-2}^{k+1} + 4\,p_{\nu-1}^{k+1} - 3\,p_\nu^{k+1}}{2\,\Delta\xi} \tag{5}$$

[1] The spatial step size $\Delta\xi$ is assumed to be chosen such that $l/\Delta\xi \in \mathbb{N}$.

by approximating (2) using a second-order difference quotient and by taking into account that $q_i(t)$ and $q_e(t)$ are constant in the time-interval $[t_k, t_{k+1})$. Obviously, Equations (3), (4), and (5) can be summarized in the matrix equation

$$\Psi(\boldsymbol{\kappa}^{k+1})\,\boldsymbol{p}^{k+1} = \Phi(\boldsymbol{\kappa}^{k+1})\,\boldsymbol{p}^{k+1} + \Upsilon(\boldsymbol{\kappa}^{k+1})\,\boldsymbol{q}^k, \tag{6}$$

where $\Psi, \Phi \in \mathbb{R}^{(\nu+1)\times(\nu+1)}$, $\Upsilon \in \mathbb{R}^{(\nu+1)\times 2}$, and

$$\boldsymbol{\kappa}^k := \begin{pmatrix} \kappa_0^k \\ \vdots \\ \kappa_\nu^k \end{pmatrix}, \quad \boldsymbol{p}^k := \begin{pmatrix} p_0^k \\ \vdots \\ p_\nu^k \end{pmatrix}, \quad \text{and} \quad \boldsymbol{q}^k := \begin{pmatrix} q_{\text{in}}^k \\ q_{\text{ex}}^k \end{pmatrix}.$$

2.3 Fracturing and seismic events

Hydraulic stimulation can cause seismic events (see, e.g, [2]). The occurrence of an injection-induced seismic event is generally understood to result from a reduction of the effective normal stress due to the increase in fluid pressure on pre-existing faults to the point where their stress states reaches the critical condition for frictional failure (cf. [4]). We discretize the shear stress profile using the same spatial grid as for the discretization of the diffusion equation. We associate the shear stress $\tau_j^k := \tau(\xi_j, t_k)$ with every point on the discretization grid. Now, a seismic event occurs around a grid point, if the condition

$$\mu\,(\sigma - p_j^k) < \tau_j^k \tag{7}$$

holds, where μ is the friction coefficient and where σ denotes the (constant) normal stress (cf. [4, Eq. (1)]). A seismic event is assumed to have two side effects. First, the stress field will locally change. More precisely, the stress τ_j^k will be reduced by an uncertain amount $\Delta\tau$ and some of the released stress will be transferred to neighboring regions. Second, the permeability κ_j^k will be increased by a factor $(1+\epsilon)$, where the rate ϵ is again uncertain. The stress transfer may cause elements to satisfy condition (7) although we initially found $\mu\,(\sigma - p_j^k) \geq \tau_j^k$. This behavior may lead to chain reactions and thus may result in major seismic events (see [7] for details). Formally, the shear stress and permeability update from time t_k to t_{k+1} is described by the following algorithm inspired by the procedure in [4, Sect. 3].

Algorithm 1: *Pressure, stress and permeability update.*

1. *Set* $\mathcal{J} \leftarrow \emptyset$, $\boldsymbol{\kappa}^{k+1} \leftarrow \boldsymbol{\kappa}^k$, *and* $\boldsymbol{\tau}^{k+1} \leftarrow \boldsymbol{\tau}^k$.
2. *Generate* $\epsilon \sim \mathcal{N}(\hat{\epsilon}, \varsigma_\epsilon^2)$ *and* $\Delta\tau \sim \mathcal{N}(\Delta\hat{\tau}, \varsigma_{\Delta\tau}^2)$.
3. *Repeat the following steps until* $\Delta\mathcal{J} = \emptyset$.
   (a) *Set* $\Delta\mathcal{J} \leftarrow \{j \in \mathbb{N}_{[0,\nu]} \setminus \mathcal{J} \mid (7)\ \textit{holds}\}$.
   (b) *For every* $j \in \Delta\mathcal{J} \setminus \{0, \nu\}$, *set* $\tau_{j-1}^{k+1} \leftarrow \tau_{j-1}^{k+1} + 0.45\,\Delta\tau$, $\tau_j^{k+1} \leftarrow \tau_j^{k+1} - \Delta\tau$, *and* $\tau_{j+1}^{k+1} \leftarrow \tau_{j+1}^{k+1} + 0.45\,\Delta\tau$.
   (c) *For every* $j \in \Delta\mathcal{J} \cap \{0, \nu\}$, *set* $\tau_j^{k+1} \leftarrow \tau_j^{k+1} - 0.6\,\Delta\tau$ *and* $\tau_{|j-1|}^{k+1} \leftarrow \tau_{|j-1|}^{k+1} + 0.45\,\Delta\tau$.
   (d) *For every* $j \in \Delta\mathcal{J}$, *set* $\kappa_j^{k+1} \leftarrow (1+\epsilon)\,\kappa_j^{k+1}$.
   (e) *Set* $\mathcal{J} \leftarrow \mathcal{J} \cup \Delta\mathcal{J}$.
4. *Set* $s^{k+1} \leftarrow |\mathcal{J}|$ *and compute* $\mathbf{p}^{k+1}$ *according to* (6).

Step 3.(b) describes the stress transfer. Similar to [4, Fig. 4], we assume that $90\% = 2 \cdot 45\%$ of the stress reduction $\Delta\tau$ is transferred to neighboring regions. Step 3.(c) uses

an adapted stress transfer to account for boundary effects. Now, after evaluating step 3 in Algorithm 1, the set $\mathcal{J}$ contains the indices j of all locations ξ_j, where seismic events occur in the time interval $[t_k, t_{k+1})$. The seismic moment roughly is proportional to the slip-plane area (see, e.g., [4, Eq. (2)]). Thus, in our model, $|\mathcal{J}|$ provides a measure of the strength of the seismic event, which we store in the variable $s^k := s(t_k)$.

2.4 Model parameters

The values for the various model parameters (see Table 2) are not chosen to represent a specific geothermal site. However, the assumed size and depth of the reservoir, the stress field, and the rock and fluid parameters roughly match the conditions at Soultz-sous-Forêts (cf. [4, Tab. 2]). Finally note that the spatial step size satisfies the condition in footnote 1. In fact, we have $\nu = {}^{l}/_{\Delta\xi} = 120$.

Table 2: Model parameters.

Parameter	Symbol	Value	Unit
length of the reservoir	l	600	m
cross section of the reservoir	S	5000	m^2
storage coefficient	ζ	10^{-9}	${}^{1}/_{\mathrm{Pa}}$
fluid viscosity	η	$2.4 \cdot 10^{-4}$	Pa s
initial rock permeability	κ^*	$2 \cdot 10^{-14}$	m^2
initial fluid pressure	p^*	48	MPa
temporal step size	Δt	5	s
spatial step size	$\Delta\xi$	5	m
normal stress	σ	79	MPa
friction coefficient	μ	0.8	1
permeability update	$\hat{\epsilon}$	0.02	1
permeability update uncertainty	ς_ϵ	0.002	1
shear stress update	$\Delta\hat{\tau}$	0.8	MPa
shear stress update uncertainty	$\varsigma_{\Delta\tau}$	0.02	MPa

3 Model analysis

The model introduced in Sect. 2 can be understood as a nonlinear state space model with uncertainty. In fact, introducing the state and input vectors

$$x(t_k) = \begin{pmatrix} \boldsymbol{p}^k \\ \boldsymbol{\kappa}^k \\ \boldsymbol{\tau}^k \\ s^k \end{pmatrix} \in \mathbb{R}^{364} \quad \text{and} \quad u(t_k) = \boldsymbol{q}^k \in \mathbb{R}^2,$$

respectively, the transition from $x(t_k)$ to $x(t_{k+1})$ can be written as

$$x(t_{k+1}) = f(x(t_k), u(t_k), v(t_k)), \tag{8}$$

where v represents the uncertain variables ϵ and $\Delta\tau$ from step 2 in Algorithm 1. The function f is in general not differentiable (due to the switching behavior of the system). Furthermore, the pressure control in Section 4 only accounts for the pressures at the

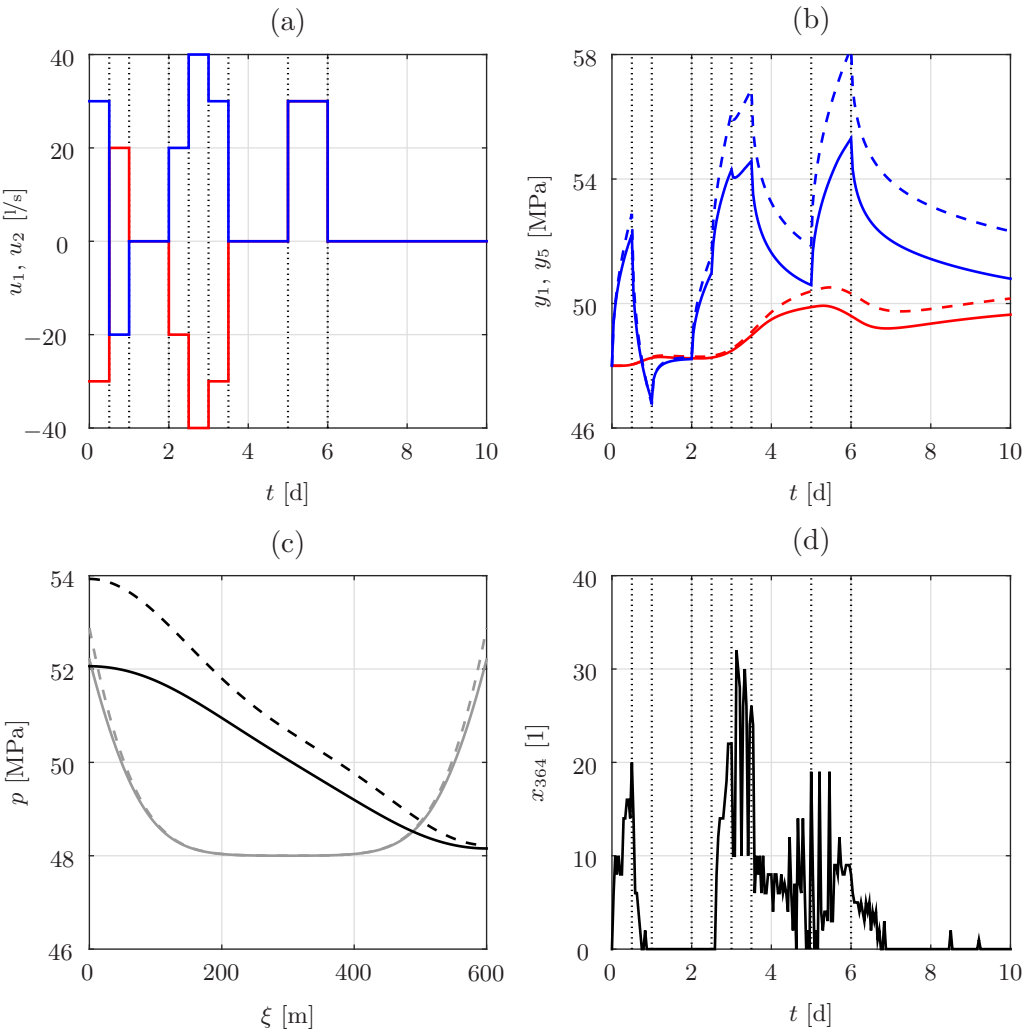

Figure 2: Illustration of (a) inputs, (b) related outputs, (c) pressure profiles, and (d) the seismic activity of the introduced models. In (a), the injected and extracted flow rates $u_1 = q_i$ (blue) and $u_2 = q_e$ (red) are shown, respectively. In (b), the pressures y_1 (blue) and y_5 (red) for the nonlinear (solid) and linear (dashed) model are illustrated. In (c), $p(\xi, t)$ is shown for $t = 12\,\mathrm{h}$ (gray) and $t = 7\,\mathrm{d}$ (black) for the nonlinear (solid) and linear (dashed) model. In (d), the strongest seismic events per hour are illustrated.

locations $\xi_{20(i-1)+1}$ with $i \in \mathbb{N}_{[1,7]}$. We thus introduce the system output $y(t_k) = C_y\, x(t_k)$ with $C_y := \sum_{i=1}^{7} e_i\, \varepsilon_{20(i-1)+1}^T \in \mathbb{R}^{7\times 364}$, where $e_i \in \mathbb{R}^7$ and $\varepsilon_j \in \mathbb{R}^{364}$ are Cartesian unit vectors. Note that y_1 and y_7 refer to the pressures in the wells, i.e., at $\xi = 0\,\mathrm{m}$ and $\xi = 600\,\mathrm{m}$. The nonlinear uncertain system becomes linear and deterministic if steps 2 and 3 are skipped in Algorithm 1. In this case, f from (8) can be rewritten as

$$f(x, u, v) = A\, x + B\, u \tag{9}$$

with appropriate matrices $A \in \mathbb{R}^{364\times 364}$ and $B \in \mathbb{R}^{364\times 2}$ (to be specified further below). We will make use of the linear approximation[2] to predict the system behavior within the MPC in Section 4. As a preparation, we analyze the response of the nonlinear system and

[2] Clearly, only the states related to the pressures $\boldsymbol{p}^k$ change in the linear model. We can thus eliminate the remaining $364 - 121 = 243$ states without loosing information. This observation is, however, only important for the numerical evaluation of the MPC in Section 4.

the linear approximation for the inputs in Figure 2.(a). We obviously have $u_1(t) = -u_2(t)$ for every $t \in [0\,\mathrm{d}, 5\,\mathrm{d}]$ and $u_1(t) = u_2(t)$ for every $t \in (5\,\mathrm{d}, 10\,\mathrm{d}]$.

The evolution of the pressures y_1 and y_5 at $\xi = 0\,\mathrm{m}$ and $\xi = 400\,\mathrm{m}$ are qualitatively comparable for the nonlinear model with uncertainty and the linear deterministic one (see Figs. 2.(b) and 2.(c)). More important, both models show typical characteristics of EGS. In fact, the pressure y_1 at the injection reacts immediately and intensely to changes of the flow rate. In contrast, the pressure y_5 in the reservoir (at $\xi = 400\,\mathrm{m}$) shows a delayed and damped reaction due to diffusion. Moreover, the largest seismic event occurs (shortly) *after* the time interval $[60\,\mathrm{h}, 72\,\mathrm{h}]$ with the highest injection rate (see Fig. 2.(d)). This so-called post-injection seismicity (see, e.g., [4, Sect. 5.4]) is typical for hydraulic stimulations in EGS.

4 Predictive pressure control

We now introduce the predictive control scheme to regulate the fluid pressure in the deep geothermal system. In particular, we intend to control the system such that

$$\lim_{t\to\infty} y_2(t) = \breve{y}_2 \quad \text{and} \quad \lim_{t\to\infty} y_5(t) = \breve{y}_5, \tag{10}$$

where $\breve{y}_2$ and $\breve{y}_5$ are reference values for the pressures at $\xi = 100\,\mathrm{m}$ and $\xi = 400\,\mathrm{m}$, respectively. Thereby, input and output constraints of the form $\underline{u} \leq u(t) \leq \overline{u}$ and $\underline{y} \leq y(t) \leq \overline{y}$ should be satisfied (at least point-wise in time). The described control task does not exactly match the situation in practical application. In fact, we are mainly interested in presenting a first approach for predictive pressure control in deep geothermal systems. We stress, however, that the control scheme can be easily adapted to similar control tasks.

4.1 MPC with linear prediction

The control task can be intuitively formulated in the framework of MPC. The associated OCP may, however, be hard to solve for naive implementations. First, the usage of the nonlinear uncertain model to predict the system behavior results in a non-convex OCP. Second, the high number of states implies a high number of equality constraints (which could, of course, be eliminated). Third, the slow dynamics of the system require long prediction horizons resulting in a high number of decision variables.

We make some simplifications to facilitate the numerical solution of the OCP. First, we use a linear approximation of the nonlinear prediction model. Regarding the analysis in Section 3, this simplification is justifiable for moderate prediction horizon lengths. Second, we apply a quadratic performance index. As a consequence, the OCP can be rewritten as a quadratic program (QP). Third, we (later) eliminate equality constraints to reduce the number of constraints. Fourth, we employ move blocking strategies (see, e.g., [8]) to reduce the number of decision variables. In particular, we assume that the inputs only change every $M \in \mathbb{N}$ time steps (i.e., $u(t_{Mi+k}) = u(t_{Mi})$ for every $i \in \mathbb{N}$ and $k \in \mathbb{N}_{[1,M-1]}$). Moreover, we require the output constraints to be fulfilled only at the times t_{Mi} for $i \in \mathbb{N}$.

In summary, we consider the MPC scheme

$$
\begin{aligned}
V(x^*) := \min_{\boldsymbol{u},\boldsymbol{x},\boldsymbol{y}} & \sum_{i=1}^{N_y} \|y(t_{Mi}) - \breve{y}\|_Q^2 + \sum_{i=0}^{N_u-1} \|u(t_{Mi}) - \breve{u}\|_R^2 && (11)\\
\text{s.t.} \quad & x(t_0) = x^*, \\
& x(t_{k+1}) = A^* x(t_k) + B^* u(t_k), && \forall k \in \mathbb{N}_{[0,MN_y-1]}, \\
& y(t_{Mi}) = C_y\, x(t_{Mi}), && \forall i \in \mathbb{N}_{[1,N_y]}, \\
& u(t_{Mi}) = u(t_{M(N_u-1)}), && \forall i \in \mathbb{N}_{[N_u,N_y-1]}, \\
& u(t_{Mi+k}) = u(t_{Mi}), \qquad \forall i \in \mathbb{N}_{[0,N_y-1]}, && \forall k \in \mathbb{N}_{[1,M-1]}, \\
& \underline{u} \le u(t_{Mi}) \le \overline{u}, && \forall i \in \mathbb{N}_{[0,N_u-1]}, \\
& \underline{y} \le y(t_{Mi}) \le \overline{y}, && \forall i \in \mathbb{N}_{[1,N_y]},
\end{aligned}
$$

where N_y and N_u refer to the output and input prediction horizon, respectively. The positive (semi-) definite matrices Q and R determine the output and input weights. The vector $\breve{u} \in \mathbb{R}^2$ defines the input reference. The value $V(x^*)$ is the optimal cost for the initial condition x^* and

$$
\boldsymbol{u} := \begin{pmatrix} u(t_0) \\ u(t_1) \\ \vdots \\ u(t_{MN_y-1}) \end{pmatrix}, \quad \boldsymbol{x} := \begin{pmatrix} x(t_0) \\ x(t_1) \\ \vdots \\ x(t_{MN_y}) \end{pmatrix}, \quad \boldsymbol{y} := \begin{pmatrix} y(t_M) \\ y(t_{2M}) \\ \vdots \\ y(t_{MN_y}) \end{pmatrix}
$$

denote the decision variables of the OCP. Finally, inspired by (6) and (9), the linearization around x^* is described by

$$
A^* := \begin{pmatrix} \Psi^{-1}(\boldsymbol{\kappa}^*)\, \Phi(\boldsymbol{\kappa}^*) & 0 \\ 0 & I_{243} \end{pmatrix} \text{ and } B^* := \begin{pmatrix} \Psi^{-1}(\boldsymbol{\kappa}^*)\, \Upsilon(\boldsymbol{\kappa}^*) \\ 0 \end{pmatrix},
$$

where $\boldsymbol{\kappa}^* := \begin{pmatrix} x^*_{122} & \dots & x^*_{242} \end{pmatrix}^T$. Now, by eliminating all equality constraints according to the procedure in [9], (11) can be equivalently rewritten as the QP

$$
\begin{aligned}
V(x^*) = \min_{\boldsymbol{z}} \; & \frac{1}{2}\, \boldsymbol{z}^T H\, \boldsymbol{z} + (Gx^* + g)^T \boldsymbol{z} + \|Fx^* + c\|_2^2 && (12)\\
\text{s.t.} \quad & E\, \boldsymbol{z} \le D\, x^* + d
\end{aligned}
$$

with appropriate matrices (and vectors) H, G, g, F, E, D, d, and c (see [9] for details) and the decision variables

$$
\boldsymbol{z} := \begin{pmatrix} u(t_0) \\ u(t_M) \\ \vdots \\ u(t_{M(N_u-1)}) \end{pmatrix} \in \mathbb{R}^{2N_u}. \tag{13}
$$

During runtime of the controller, the OCP (12) (or, alternatively (11)) is repeatedly solved for the current state x^* and the first input of the optimal input sequence is applied to the system. Formally, this procedure leads to the control law

$$
\varrho(x^*) := u^*(t_0),
$$

where $u^*(t_0)$ is the first entry of the optimizer $\boldsymbol{z}^*$ for (12) at x^*.

It remains to specify the choice of the weighing matrices and the reference signals. Regarding the control task in (10), the choice $Q = e_2\, e_2^T + e_5\, e_5^T \in \mathbb{R}^{7\times 7}$ is suitable to penalize deviations from the output references $\breve{y}_2$ and $\breve{y}_5$. Clearly, this choice of Q implies that the deviations $y_j(t) - \breve{y}_j$ for $j \in \mathbb{N}_{[1,7]} \setminus \{2,5\}$ do not influence the performance index. Consequently, $\breve{y} := \breve{y}_2\, e_2 + \breve{y}_5\, e_5 \in \mathbb{R}^7$ is a suitable choice for the output reference. An appropriate choice for the input reference requires some preparation. Obviously, the inputs $\breve{u}$ should support stationarity of the system if $y_2(t^*) = \breve{y}_2$ and $y_5(t^*) = \breve{y}_5$ hold for some $t^* \in \mathbb{R}_+$. From (1), we infer that stationarity requires

$$0 = \frac{\partial^2 p(\xi, t^*)}{\partial \xi^2} \qquad \text{for every} \qquad \xi \in [0, l], \tag{14}$$

which can only be fulfilled if $p(\xi, t^*)$ is affine. By definition of the system outputs y, we have $y_2(t^*) = p(100, t^*)$ and $y_5(t^*) = p(400, t^*)$. Thus, the affine pressure profile is uniquely defined by $\breve{y}_2$ and $\breve{y}_5$. In fact, $p(\xi, t^*)$ can be written as $p(\xi, t^*) = a\,\xi + b$ with

$$a := \frac{\breve{y}_5 - \breve{y}_2}{300} \qquad \text{and} \qquad b := \frac{4\,\breve{y}_2 - \breve{y}_5}{3}.$$

We thus require the injection and extraction flow rates

$$q_{\text{in}}(t^*) = -\frac{S\,a}{\eta}\,\kappa(0, t^*) \quad \text{and} \quad q_{\text{ex}}(t^*) = -\frac{S\,a}{\eta}\,\kappa(l, t^*)$$

to ensure stationarity (see (2)). Now, assuming that the permeability does not change in the future (which is, by definition, true for a stationary state), we choose the input references

$$\breve{u}_1 := -\frac{S\,a}{\eta}\,x^*_{122} \qquad \text{and} \qquad \breve{u}_2 := -\frac{S\,a}{\eta}\,x^*_{242} \tag{15}$$

depending on the current state x^*. Finally, we choose the input weighting $R = r\,I_2$, where $r \in \mathbb{R}_+$ is a tuning parameter.

4.2 UKF with nonlinear prediction

The application of the introduced MPC scheme requires (an estimation of) the current system state x^*. Clearly, measuring the complete profiles of pressure, permeability, and shear stress in the reservoir is not feasible. In fact, very few measurements can be realized in practice. Here, we assume that the fluid pressures in both wells, i.e., $p(\xi_0, \cdot) = x_1$ and $p(\xi_\nu, \cdot) = x_{121}$ can be measured. Moreover, we assume that the current magnitude of the seismic events is accessible via $s = x_{364}$. This assumption is reasonable since the induced seismicity is usually tracked during hydraulic stimulations (see, e.g., [4, Sect. 2]). All measurements are, however, effected by (white) noise. Specifically, we assume that the measurements $m(t_k) \in \mathbb{R}^3$ at time t_k are described by

$$m(t_k) = C_m\, x(t_k) + w(t_k)$$

where $C_m := e_1\, \varepsilon_1^T + e_2\, \varepsilon_{121}^T + e_3\, \varepsilon_{364}^T \in \mathbb{R}^{3\times 364}$ and where $w_1 \sim \mathcal{N}(0, \varsigma_p^2)$, $w_2 \sim \mathcal{N}(0, \varsigma_p^2)$, and $w_3 \sim \mathcal{N}(0, \varsigma_s^2)$.

Many methods exist that compute an estimate $\hat{x}^*$ of the current state x^* given an estimation of the former state $\hat{x}^-$, the former input u^-, and the current (noisy) measurement m^*. Here, we design a UKF (see, e.g., [10] or [11]) to observe the system state. The UKF is capable of handling nonlinear uncertain systems with non-differentiable functions f. Moreover, it can be applied to large scale systems since the estimation procedure builds

on a small number of test (or sigma) points (compared to particle filters). It is thus a well-suited choice for the system described in Section 2. To handle the uncertainties, the UKF exploits information on the distribution of the uncertain variables. In particular, we require (estimations of) the mean $\hat{v}$ and the covariance matrix P_{vv} of the process uncertainty v as well as the covariance matrix P_{ww} of the measurement noise. Obviously, based on the assumed distributions of v and w, we have $\hat{v} = \begin{pmatrix}\hat{\epsilon} & \Delta\hat{\tau}\end{pmatrix}^T$, $P_{vv} = \operatorname{diag}(\varsigma_\epsilon^2, \varsigma_{\Delta\tau}^2)$, and $P_{ww} = \operatorname{diag}(\varsigma_p^2, \varsigma_p^2, \varsigma_s^2)$. The UKF can now be implemented according to Algorithm 2, which is based on [10, Box 3.1] and [11, Alg. 3.1]. As a preparation, we define the weighting coefficients

$$\beta_0 := \frac{\lambda}{366+\lambda} \qquad \text{and} \qquad \beta_i := \frac{1}{2\,(366+\lambda)} \tag{16}$$

for every $i \in \mathbb{N}_{[1,732]}$ and some $\lambda \in \mathbb{R}$ (with $\lambda \neq -366$). Thereby, $366 = 364 + 2$ refers to the dimension of the augmented state vector that concatenates the original state and the process noise (see [10, Eq. (15)]). In addition to the weighting coefficients, we precalculate the v coordinates[3] of the $733 = 2 \cdot 366 + 1$ sigma points according to $\mathcal{V}_i := \hat{v}$ for every $i \in \mathbb{N}_{[0,728]}$ as well as

$$\begin{aligned}\mathcal{V}_{728+i} &:= \hat{v}^- + \sqrt{366+\lambda}\, e_i^T L_v \qquad \text{and}\\ \mathcal{V}_{730+i} &:= \hat{v}^- - \sqrt{366+\lambda}\, e_i^T L_v\end{aligned}$$

for every $i \in \{1, 2\}$, where $L_v := \operatorname{diag}(\varsigma_\epsilon, \varsigma_{\Delta\tau})$. Note that L_v obeys $L_v L_v^T = P_{vv}$. Now, Algorithm 2 first computes the x coordinates of the 733 sigma points. In step 2, the nonlinear model is used to compute state and output predictions for every sigma point (with the components $\mathcal{X}_i^-$ and $\mathcal{V}_i$). In step 3 and 4, these predictions are used to calculate the expectations for the current state and output, and the covariance matrices $\tilde{P}_{xx}$, P_{xm}, and P_{mm}, respectively. Finally, in step 5, the filter gain W is computed, which is used to adapt the estimations for the current state and the associated covariance matrix.

Algorithm 2: *UKF implementation.*

1. *Compute L_x such that $L_x L_x^T = P_{xx}^-$ and set sigma points.*
   (a) *For every $i \in \{0\} \cup \mathbb{N}_{[729,732]}$, set $\mathcal{X}_i^- \leftarrow \hat{x}^-$.*
   (b) *For every $i \in \mathbb{N}_{[1,364]}$, set $\mathcal{X}_i^- \leftarrow \hat{x}^- + \sqrt{366+\lambda}\,\varepsilon_i^T L_x$ and $\mathcal{X}_{364+i}^- \leftarrow \hat{x}^- - \sqrt{366+\lambda}\,\varepsilon_i^T L_x$.*
2. *For every $i \in \mathbb{N}_{[0,732]}$, compute predictions $\mathcal{X}_i \leftarrow f(\mathcal{X}_i^-, u^-, \mathcal{V}_i)$ and $\mathcal{M}_i \leftarrow C_m\,\mathcal{X}_i$.*
3. *Compute $\tilde{x} \leftarrow \sum_{i=0}^{732} \beta_i \mathcal{X}_i$ and $\tilde{m} \leftarrow \sum_{i=0}^{732} \beta_i \mathcal{M}_i$.*
4. *Compute approximations of covariance matrices.*
   (a) *$\widetilde{P}_{xx} \leftarrow \sum_{i=0}^{732} \beta_i (\mathcal{X}_i - \tilde{x})\,(\mathcal{X}_i - \tilde{x})^T$.*
   (b) *$P_{xm} \leftarrow \sum_{i=0}^{732} \beta_i (\mathcal{X}_i - \tilde{x})\,(\mathcal{M}_i - \tilde{m})^T$.*
   (c) *$P_{mm} \leftarrow P_{ww} + \sum_{i=0}^{732} \beta_i (\mathcal{M}_i - \tilde{m})\,(\mathcal{M}_i - \tilde{m})^T$.*
5. *Compute filter gain $W \leftarrow P_{xm}\,P_{mm}^{-1}$ and set $\hat{x}^* \leftarrow \tilde{x} + W(m^* - \tilde{m})$ and $P_{xx} \leftarrow \widetilde{P}_{xx} - W P_{mm} W^T$.*

We refer to [10] and [11] for details on the implementation of UKF. We stress, however, that the choice of the weighting coefficients in (16) refers to the *unscaled* unscented transformation as introduced in [10, Eq. (12)]. The performance of the UKF can often

[3] Neglecting a potential covariance between the state estimation and the process uncertainty, the sigma points in the augmented space can be computed independently in the x and v coordinates.

be improved by considering the *scaled* unscented transformation as discussed in [12] and applied in [11, Eq. (15)]. Here, we do not make use of this improvement in order to keep the number of observer parameters at a minimum (i.e., only λ).

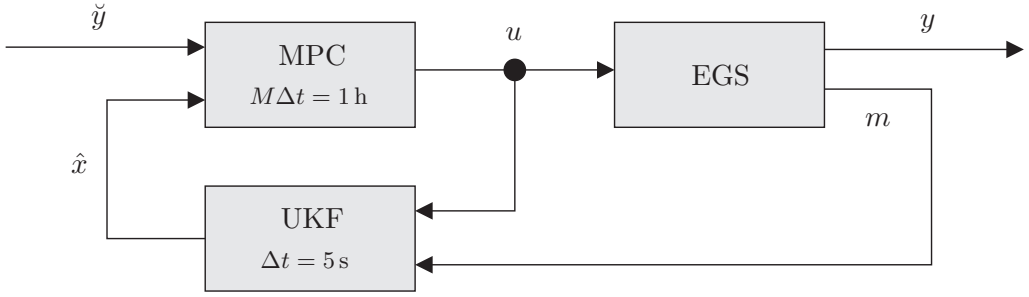

Figure 3: Schematic illustration of the control loop consisting of the geothermal system with underground reservoir and well doublet (i.e., the EGS), the controller (i.e., the MPC), and the observer (i.e., the UKF). The listed periods refer to sampling times of the controller and the observer.

4.3 Combination and simulation

We briefly explain the combination of the controller (i.e., the MPC) and the observer (i.e., the UKF) for the system of interest (i.e., the EGS). The MPC generates the input u based on the output reference, the (current) input reference, and the estimation of the current system state (see Fig. 3). Note that, according to (15), the input reference is not a design parameter since it depends on (an approximation of) the current system state. Now, the UKF estimates $\hat{x}$ based on the input u and the (noisy) measurements m (see Alg. 2). The sampling time of the observer is chosen to equal the temporal step size Δt of the model. In contrast, the controller is only evaluated every M time steps following the move blocking strategy in Section 4.1.

Table 3: Controller and observer parameters.

Parameter	Symbol	Value	Unit
first reference pressure	$\breve{y}_2$	57	MPa
second reference pressure	$\breve{y}_5$	50	MPa
output prediction horizon	N_y	72	1
input prediction horizon	N_u	24	1
maximum injection rate	$\overline{u}_1$	40	$^1/_\mathrm{s}$
minimum injection rate	$\underline{u}_1$	-30	$^1/_\mathrm{s}$
maximum production rate	$\overline{u}_2$	30	$^1/_\mathrm{s}$
minimum production rate	$\underline{u}_2$	-40	$^1/_\mathrm{s}$
maximum pressure	$\overline{y}_1, \ldots, \overline{y}_7$	70	MPa
minimum pressure	$\underline{y}_1, \ldots, \underline{y}_7$	44	MPa
sample time multiplier	M	720	1
pressure measurement noise	ς_p	0.2	MPa
seismicity measurement noise	ς_s	0.5	1
observer parameter	λ	50	1

We implemented the controller and observer using the parameters in Tab. 3. With

$M = 720$, we obtain a controller sampling time of $M\Delta t = 1\,\mathrm{h}$. In addition, the choice $N_y = 72$ implies that the outputs are predicted for $N_y M \Delta t = 3\,\mathrm{d}$. Moreover, the input prediction horizon $N_u = 24$ sets the number of decision variables equal to 48 (see Eq. (13)). Regarding the observer, we found $\lambda = 50$ to be suitable to describe the unscented transformation. Finally, we randomly initialized the observer state $\hat{x}(t_0)$ in the hyperrectangle $[0.98, 1.02]\, x(t_0)$, i.e., with a maximal relative error of 2%.

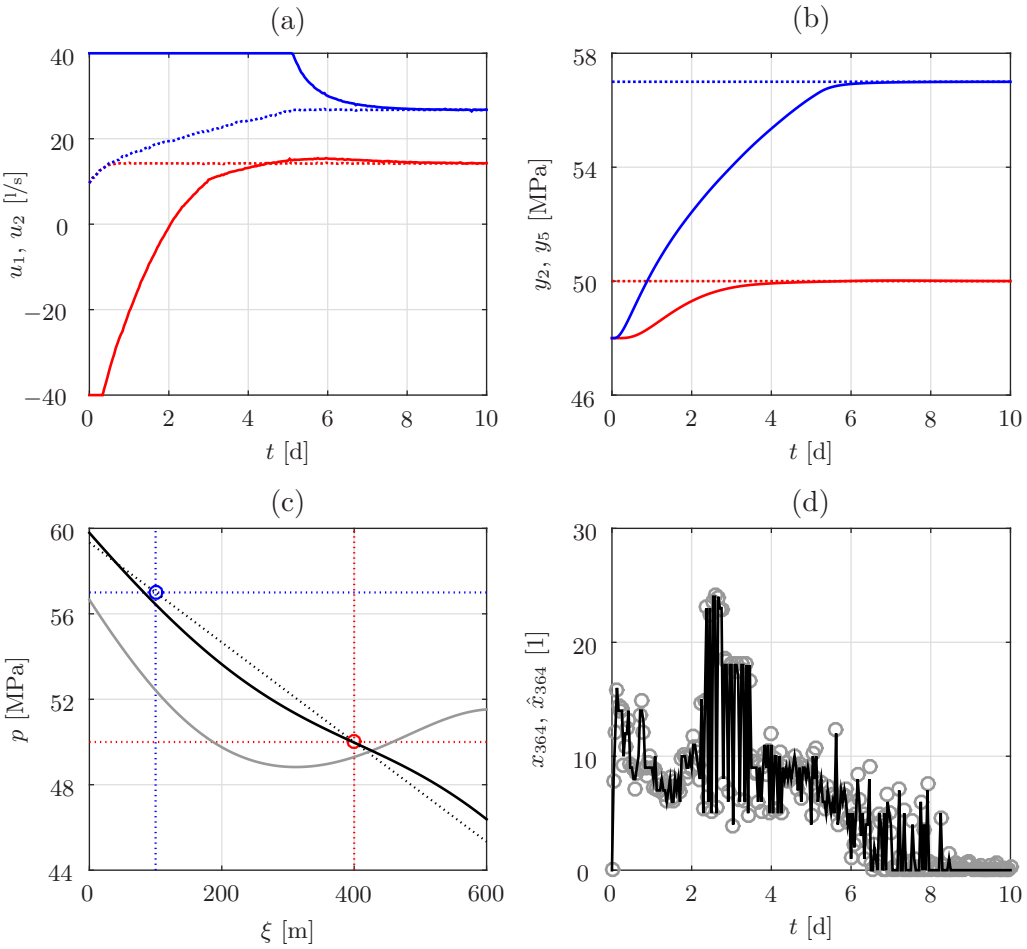

Figure 4: Illustration of (a) inputs (injection and production flow), (b) outputs (fluid pressures at $\xi = 100\,\mathrm{m}$ and $\xi = 400\,\mathrm{m}$), (c) pressure profiles, and (d) the seimic activity of the controlled system. In (a), the computed inputs $u_1 = q_{\mathrm{in}}$ (blue, solid) and $u_2 = q_{\mathrm{ex}}$ (red, solid) are shown. The dotted curves refer to the (time-dependent) input references according to (15). In (b), the controlled outputs y_2 (blue, solid) and y_5 (red, solid) are illustrated. The dotted lines depict the output references $\breve{y}_2$ and $\breve{y}_5$. In (c), $p(\xi, t)$ is shown for $t = 2\,\mathrm{d}$ (gray, solid) and $t = 5\,\mathrm{d}$ (black, solid). The dotted lines indicate the reference pressures $\breve{y}_2$ (blue) and $\breve{y}_5$ (red) as well as the affine pressure profile $a\,\xi + b$ (black). In (d), the strongest seismic events per hour are illustrated. Gray circles refer to quantities estimated by the observer.

The resulting control scheme is capable of solving the considered control task (see Figs. 4.(a) and 4.(b)). The reference pressures are matched after $t \approx 6\,\mathrm{d}$ without violating the input and state constraints. Moreover, as expected, the pressure profile tends to the affine profile determined by $\breve{y}_2$ and $\breve{y}_5$ for $t \to \infty$ (see Fig. 4.(c)). As apparent from Fig. 4.(d), the state transition causes a number of seismic events. Since seismicity

involves permeability increases, the hydraulic diffusity is permanently changing. These (inhomogeneous) changes in the permeability also explain that the injected and extracted fluid flows do not match for $t \to \infty$. In fact, taking the reference inputs (15) into account, the mismatch is obviously caused by different permeabilities around the injection and production well.

5 Conclusions and Outlook

We presented a predictive control scheme for the regulation of the fluid pressure profile in deep geothermal systems during hydraulic stimulation. The MPC builds on a rudimentary model (inspired by [4]) describing the pressurization and seismicity in the reservoir. Since only the fluid pressure in the two wells as well as the seismic activity can be measured directly, a UKF was designed to solve the observation problem. Numerical simulations showed the effectiveness of the approach.

During hydraulic stimulations of reservoir rocks, one intends to avoid strong seismic events since geothermal sites are often located in the proximity of populated areas. Controlling the fluid pressure profile in the reservoir is a first step in this direction. Nevertheless, future work has to address the explicit inclusion of seismic activity in the predictive control scheme. This extension is non-trivial, since the linear approximation (currently used in the MPC), does not incorporate seismicity. Clearly, the nonlinear uncertain model can instead be used to predict the system behavior. However, doing so leads to a large-scale non-convex OCP that we cannot solve efficiently so far.

Acknowledgment

Partial funding by the German Research Foundation (DFG) under the grants SCHU 2094/1-1 and SCHU 2094/2-1 is gratefully acknowledged.

References

[1] R. Bertani, "Geothermal power generation in the world 2010–2014 update report," in *Proc. of the World Geothermal Congress 2015*, 2015.

[2] A. McGarr, "Maximum magnitude earthquakes induced by fluid injection," *J. Geophys. Res. Solid Earth*, vol. 119, pp. 1008–1019, 2014.

[3] J. J. Bommer, S. Oates, J. M. Cepeda, C. Lindholm, J. Bird, R. Torres, G. Marroquín, and J. Rivas, "Control of hazard due to seismicity induced by a hot fractured rock geothermal project," *Engineering Geology*, vol. 83, pp. 287–306, 2006.

[4] S. Baisch, R. Vörös, E. Rothert, H. Stang, R. Jung, and R. Schellschmidt, "A numerical model for fluid injection induced seismicity at Soultz-sous-Fôret," *International Journal of Rock Mechanics and Mining Sciences*, vol. 47, pp. 405–413, 2010.

[5] J. Bear, *Dynamics of Fluids in Porous Media*. Dover Publications, 1972.

[6] J. Renner and H. Steeb, "Modeling of fluid transport in geothermal research," in *Handbook of Geomathematics*. Springer, 2014, pp. 1–55.

[7] P. Bak and C. Tang, "Earthquakes as a self-organized critical phenomenon," *Journal of Geophysical Research*, vol. 94, no. B 11, pp. 15 635–15 637, 1989.

[8] R. Cagienard, P. Grieder, E. C. Kerrigan, and M. Morari, "Move blocking strategies in receding horizon control," in *Proc. of 43rd IEEE Conference on Decision and Control*, 2004, pp. 2023–2028.

[9] A. Bemporad, M. Morari, V. Dua, and E. N. Pistikopoulos, "The explicit linear quadratic regulator for constrained systems," *Automatica*, vol. 38, no. 1, pp. 3–20, 2002.

[10] S. J. Julier and J. K. Uhlmann, "New extension of the Kalman filter to nonlinear systems," in *Proc. of the 11th Symposin on Aerospace / Defence Sensing, Simulation, and Controls*, 1997.

[11] E. A. Wan and R. Van Der Merwe, "The unscented Kalman filter for nonlinear estimation," in *Proc. of the IEEE Adaptive Systems for Signal Processing, Comm., and Cont. Symposium*, 2000, pp. 153–158.

[12] S. J. Julier, "The scaled unscented transformation," in *Proc. of the American Control Conference*, 2002, pp. 4555–4559.